Spin-orbit and orbit-spin conversion in the sharp focus of laser light: Theory and experiment

V. V. Kotlyar, A. G. Nalimov, A. A. Kovalev, A. P. Porfirev, and S. S. Stafeev
Image Processing Systems Institute of RAS–Branch of the FSRC "Crystallography and Photonics" RAS, Samara 443001, Russia and Samara National Research University, Samara 443086, Russia

(Received 16 June 2020; revised 31 July 2020; accepted 17 August 2020; published 1 September 2020)

Based on the Richards-Wolf theory, it is strictly shown that in the sharp focus of a linearly polarized laser beam, the flux of a spin vector has only transverse components (the effect of photonic wheels or a photonic helicopter). For a linearly polarized optical vortex, the orbit-spin conversion leads to the appearance of both longitudinal and transverse components of the spin angular momentum (SAM) vector in the focus. We show that in the strong focus of a circularly polarized Gaussian beam, the longitudinal component of the SAM is maximal on the optical axis, with the longitudinal component of the orbital angular momentum (OAM) being maximal on a ring. In this way, the effect of SAM and OAM on the motion of a trapped microparticle can be evaluated separately. Spin-orbit conversion is experimentally demonstrated for a circularly polarized Gaussian beam when transverse energy flux (orbital angular momentum) arises in the focus, which is transmitted to a microparticle and causes it to rotate. Switching the handedness of circular polarization (from left to right) switches the direction of microparticle rotation. It is also shown here that an azimuthally polarized vortex beam with an arbitrary integer topological charge generates in the focus a SAM vector with only an axial component (pure magnetization), whereas there is no transverse spin flux.

DOI: 10.1103/PhysRevA.102.033502

I. INTRODUCTION

Strong focusing of laser light, where a focal spot of subwavelength size is achieved, has been a focus of optical research for some time. By way of illustration, the newly discovered optical phenomena in the subwavelength focus include optical needles [1–4], dark focal spots [5], light tunnels [6,7], chains of foci [8,9], and foci with a flat apex [10–12]. This list is not complete, and other nontrivial effects that occur in the strong focus and may have interesting and diverse applications have also been reported. On the optical axis near the focus, reverse energy flux has been discovered [13], while in the focal plane we have revealed a toroidal energy flux around the "dark rings" where the flux is zero [14]. In addition, an "angular tractor" phenomenon has been discovered when the transverse energy flux on adjacent light rings in the focal plane is directed in opposite directions (clockwise and counterclockwise) [15]. It has also been rigorously theoretically shown that in the sharp focus of a circularly polarized Gaussian beam, a spiral energy flow appears due to the spin-orbital conversion [16]. Spin-orbital conversion, and related to it the optical Hall effect and rotation of microparticles along a circular path, has also been studied in [17–20]. In recent years, a number of other novel and interesting phenomena have been discovered in studies of sharply focused vortex laser beams and beams with inhomogeneous polarization: the formation of tangles and knots from points of phase and polarization singularities [21–23], photonic wheels [24], the formation of Möbius polarization strips [25,26], and pure magnetization [27,28]. All these effects have been demonstrated numerically, and some also experimentally, but there is no rigorous analytical theory to describe them. In this work, with a unified approach, we obtain simple analytical expressions for the light-field components in the sharp focus, as well as for the spin angular momentum, Poynting vector, and orbital energy flow. These expressions clearly lead to the following phenomena: spin-orbit conversion, optical wheels, Möbius polarization topology, and pure magnetization. It is experimentally demonstrated that the orbital angular momentum, appearing in the focus of a circularly polarized Gaussian beam, causes a dielectric nonabsorbing particle to rotate around its own center of mass, located on the optical axis of the beam.

The Richards-Wolf theory [29] adequately describes all six components of the electric and magnetic vectors of an electromagnetic field near the focus. In this paper, based on this theory, we give a rigorous description of some of the above interesting phenomena. We also demonstrate experimentally the spin-orbit conversion predicted in [16], which generates the orbital angular momentum in the sharp focus of a simple Gaussian beam with circular polarization. This orbital angular momentum is transmitted to a microparticle trapped in the focus and rotates it around the optical axis (and around its center of mass). A Gaussian beam has already been used to rotate a microparticle [18,20], but along a circular path rather than around its center of mass.

Rotation of an absorbing (CuO) microparticle around its center of mass, when the particle is trapped in a light ring in the focus of a circularly polarized optical vortex with a topological charge of 3, was demonstrated in [30,31]. In contrast to [30,31], we study here a dielectric (almost nonabsorbing) microparticle, rotating around its center of mass in the intensity maximum of a sharply focused circularly polarized

Gaussian beam. In [32], using the plane-wave expansion of the electric field vector, the axial component of the angular momentum (AM) vector is represented as a sum of two terms. However, these terms are not associated in [32] with the spin AM (SAM) and orbital AM (OAM). In contrast with this work, Ref. [32] does not consider the sharp focusing of light within the Richards-Wolf formalism. In [33], the most general expressions for OAM and SAM were obtained in operator form (as average values of the corresponding operators). In particular, an expression (11) for OAM was obtained in [33] in the form of two terms, one of which is the average of the angular momentum operator, and the second is the average of the Berry-phase operator related with circular polarization. This second term in Eq. (11) from [33] is associated with spin-orbit conversion. We note, however, that [33] does not contain explicit analytical expressions for the energy flux and for the spin flux in sharp focus. In contrast to this work, Refs. [31,33] do not consider the energy and spin flows in the focus of linearly and azimuthally polarized light. Closest to this work is Ref. [34], in which an attempt was made to consider the energy flux and angular momentum in the sharp focus of an optical vortex with circular polarization. But unfortunately, Eqs. (11) and (21) are incorrect in [34]. Equation (21) from [34] incorrectly equates the energy flux (Poynting vector) with the spin flux vector. In our work, the energy flux vector [Eq. (8)], spin flux [Eq. (12)], and SAM vector [Eq. (2)] are calculated in the focus separately.

We note here that for simulation in this work we use the finite-difference method for solving the Maxwell's equations (FDTD method), implemented in the commercial software FULLWAVE (RSoft Design). This method is more accurate than the vectoral integrals in [29], which correctly describe the light field in focus if the focal length is much larger than the wavelength.

II. SPIN-ORBIT CONVERSION IN THE FOCUS

Let the initial field be a circularly polarized optical vortex with a topological charge m and with an arbitrary axisymmetric envelope function:

$$\mathbf{E} = A(\theta)e^{im\varphi}\begin{pmatrix}1\\ i\sigma\end{pmatrix}, \quad \mathbf{H} = A(\theta)e^{im\varphi}\begin{pmatrix}-i\sigma\\ 1\end{pmatrix}, \tag{1}$$

where $\sigma = 1$ stands for right-hand circular polarization, $\sigma = -1$ for left-hand circular polarization, $\sigma = 0$ for linear polarization, and $\sigma \neq 0, \ \pm 1$ for elliptical polarization (it is supposed below that σ is a real number). Spin density or SAM of the electric field (without the spin of the magnetic field taken into account) can be deduced using the known formula [35]

$$\mathbf{s}_E = \frac{1}{16\pi\omega}\mathrm{Im}(\mathbf{E}^* \times \mathbf{E}), \tag{2}$$

where ω is the cycling frequency of light. Below we omit the constant $(1/8\pi\omega)$ for brevity. Vectors $\mathbf{E}$ and $\mathbf{H}$ in Eqs. (1) and (2) are the electric and magnetic strength vectors of an electromagnetic wave. Then, according to the Richards-Wolf formalism [29], the SAM vector from Eq. (2) has the following components in the focal plane:

$$\begin{aligned}
s_{xE} &= (-\sigma\gamma_+ I_{0,m}I_{1,m+1} - \sigma\gamma_- I_{0,m}I_{1,m-1} - \gamma_+^2 I_{1,m+1}I_{2,m+2} + \gamma_-^2 I_{1,m-1}I_{2,m-2})\sin\varphi + \gamma_+\gamma_-(I_{1,m-1}I_{2,m+2} - I_{1,m+1}I_{2,m-2})\sin 3\varphi,\\
s_{yE} &= (\gamma_+ I_{0,m}I_{1,m+1} - \gamma_- I_{0,m}I_{1,m-1} + \gamma_+^2 I_{1,m+1}I_{2,m+2} - \gamma_-^2 I_{1,m-1}I_{2,m-2})\cos\varphi - \gamma_+\gamma_-(I_{1,m-1}I_{2,m+2} - I_{1,m+1}I_{2,m-2})\cos 3\varphi,\\
s_{zE} &= \sigma I_{0,m}^2 - \gamma_+^2 I_{2,m+2}^2 + \gamma_-^2 I_{2,m-2}^2 + \gamma_+\gamma_- I_{0,m}(I_{2,m-2} - I_{2,m+2})\cos 2\varphi.
\end{aligned} \tag{3}$$

In Eq. (3), we use the following designations for the integrals:

$$I_{\nu,\mu} = \left(\frac{\pi f}{\lambda}\right)\int_0^{\theta_0} \sin^{\nu+1}\left(\frac{\theta}{2}\right)\cos^{3-\nu}\left(\frac{\theta}{2}\right) \times \cos^{1/2}(\theta)A(\theta)e^{ikz\cos z}J_\mu(x)d\theta, \tag{4}$$

where f is the focal length of the aplanatic system, λ is the wavelength, $\mathrm{NA} = \sin\theta_0$ is the numerical aperture, $J_\mu(x)$ is the Bessel function of the first kind, $x = kr\sin\theta$, and (x, y, z) and (r, φ, z) are, respectively, the Cartesian and the polar coordinates. As the amplitude of the initial radial envelope function $A(\theta)$, we can use the Bessel-Gaussian function [36]:

$$A(\theta) = J_1\left(2\beta\frac{\sin\theta}{\sin\alpha}\right)\exp\left[-\beta^2\left(\frac{\sin\theta}{\sin\alpha}\right)^2\right], \tag{5}$$

where β is the pupil radius of the aplanatic system divided by the waist radius of the Gaussian beam, $\gamma_\pm = (1 \pm \sigma)/2$ (for $\sigma = 0$, other values of constants are used, $\gamma_+ = \gamma_- = 1/\sqrt{2}$). In the partial case of left-hand circular polarization ($\sigma = -1$, $\gamma_+ = 0$, $\gamma_- = 1$), Eq. (3) reduces to

$$\begin{aligned}
s_{xE-} &= Q(r)\sin\varphi, \quad s_{yE-} = -Q(r)\cos\varphi,\\
s_{zE-} &= I_{2,m-2}^2 - I_{0,m}^2, \quad Q(r) = I_{1,m-1}(I_{0,m} + I_{2,m-2}).
\end{aligned} \tag{6}$$

Equation (6) shows that the spin-density vector of an optical vortex with left-hand circular polarization has all three components in the focus. If instead of the optical vortex there is a Gaussian beam with left-hand circular polarization ($m = 0$), then in the focal plane all the spin components are still nonzero:

$$\begin{aligned}
s_{xE0-} &= -Q(r)\sin\varphi, \quad s_{yE0-} = Q(r)\cos\varphi,\\
s_{zE0-} &= I_{2,2}^2 - I_{0,0}^2, \quad Q(r) = I_{1,1}(I_{0,0} + I_{2,2}).
\end{aligned} \tag{7}$$

Due to the optical effect of spin-orbit conversion, a nonzero energy flux arises in the focus of a Gaussian beam with left-hand circular polarization [16]. Indeed, the Poynting vector (energy flux) reads [29]

$$\mathbf{S} = [c/(8\pi)]\mathrm{Re}[\mathbf{E} \times \mathbf{H}^*], \tag{8}$$

where c is the speed of light in vacuum, $\mathbf{E} \times \mathbf{H}$ is the cross product, and * stands for complex conjugation. Below, we

omit the constant $c/(8\pi)$. For the components of the Poynting vector in the focal plane of a homogeneously polarized optical vortex, we get

$$S_z = \left(\frac{1+\sigma^2}{2}\right) I_{0,m}^2 - \gamma_+^2 I_{2,m+2}^2 - \gamma_-^2 I_{2,m-2}^2, \tag{9}$$

$$S_x = -Q(r)\sin\varphi,$$

$$S_y = Q(r)\cos\varphi,$$

$$Q(r) = \gamma_+^2 I_{1,m+1}(I_{0,m} + I_{2,m+2}) + \gamma_-^2 I_{1,m-1}(I_{0,m} + I_{2,m-2}). \tag{10}$$

For a Gaussian beam with left-hand circular polarization, Eq. (10) reduces to

$$S_{z0-} = I_{0,0}^2 - I_{2,2}^2, \quad S_{x0-} = Q(r)\sin\varphi,$$
$$S_{y0-} = -Q(r)\cos\varphi, \quad Q(r) = I_{1,1}(I_{0,0} + I_{2,2}). \tag{11}$$

A comparison of Eqs. (7) and (11) indicates that in addition to the SAM (7) there is the energy flux of the same magnitude (11) in the focus. They are equal up to a sign, i.e., the transverse energy flux rotates [$S_{\varphi-} = -Q(r)$, $S_{r-} = 0$] in the opposite direction (clockwise) with respect to the direction of SAM vectors (they are directed counterclockwise). Figure 1 shows the intensity distribution [Fig. 1(a)] of a plane wave with left-hand circular polarization (i.e., polarization vectors rotate counterclockwise) in the focal plane, as well as distribution of the azimuthal component S_φ of the transverse energy flux in the focus [Fig. 1(b)] and its radial cross section [Fig. 1(c)]. The negative values of S_φ in Figs. 1(b) and 1(c) show a clockwise rotation of the Poynting vector **S** in the XY plane. Figure 1 was obtained by the FDTD method for the following parameters: wavelength $\lambda = 532$ nm, size of the cell in the computation grid $\lambda/30$, a launch plane wave is limited by an 8-μm-diam aperture, and focal length $f = 4.55\,\mu$m (numerical aperture NA = 0.65). In this work, all cases of numerical simulation are based on the FDTD-based rigorous solution of Maxwell's equations. The price to be paid for the rigorous solution is a huge amount of computations leading to a very long computing process. Because of this, we assume input beam diameters and focal lengths comparable with incident wavelengths. On the other hand, examples of zone plates [37] and microlenses [38] with focal lengths comparable with the wavelength of light have been reported.

It should be taken into consideration that the larger the focal length compared to the incident wavelength, the more accurate is the Richards-Wolf theory [29]. Because of this, the analytical relations derived in this work will be accurate in the focus of objectives whose focal length comprises millimeters or dozens of millimeters. However, if the focus is located near the surface of a zone plate [37] or a microlens [38] at a near-wavelength distance, the Richards-Wolf theory gives approximate results. In Fig. 1, a comparison is made between the computational results for the projections of the SAM vector using a rigorous FDTD method [Figs. 1(d) and 1(e)] and the Richards-Wolf formulas (3) and (4) [Figs. 1(f) and 1(g)]. From the comparison, the intensity patterns are seen to be in agreement.

As seen in Figs. 1(d) and 1(e), transverse components of the SAM vectors are directed counterclockwise. A

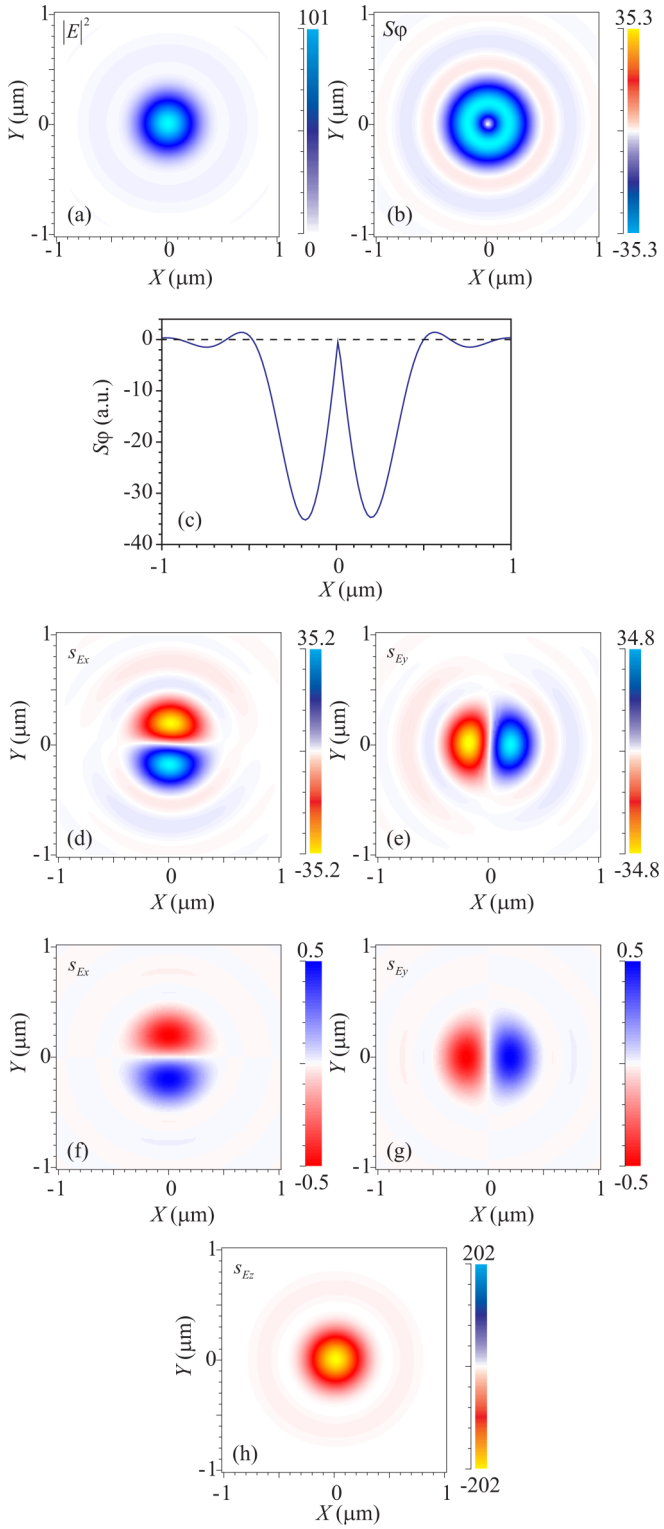

FIG. 1. Intensity distribution of the electric field component $|E|^2$ (a), azimuthal component S_φ of the Poynting vector (radial component is zero) (b), and its cross-section along the X-axis through the optical axis (c). Components of the SAM vector in the focal plane: s_{Ex} (d), (f), s_{Ey} (e), (g), and s_{Ez} (h), calculated using an FDTD method (d), (e), (h) and Richards-Wolf formulas (f), (g).

comparison of Fig. 1(b) and Figs. 1(d) and 1(e) shows that the transverse energy flux and the transverse distribution of SAM vectors are equal in magnitude and opposite

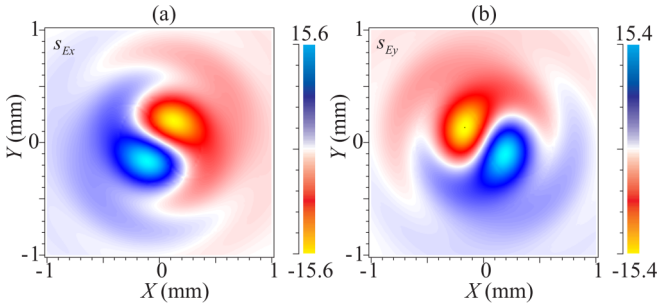

FIG. 2. Distributions of the transverse components of the spin-density vector s_{Ex} (a) and s_{Ey} (b) at a distance of 2λ beyond the focal plane when focusing a Gaussian beam with left-hand circular polarization. In Fig. 1, these distributions are shown in the focal plane: s_{Ex} [Fig. 1(d)] and s_{Ey} [Fig. 1(e)].

in sign. This is also seen from a comparison of Eqs. (7) and (11).

Figure 2 shows distributions of the transverse components of the SAM vector s_{Ex} (a) and s_{Ey} (b) at a distance of 2λ from the focal plane. It is seen that the SAM vectors rotate by a certain angle clockwise, that is, the transverse flux of the spin vector rotates in the same direction as the transverse flux of energy [Figs. 1(b) and 1(c)]. This can be explained. According to [39], energy flux consists of the spin flux and the orbital energy flux. The Gaussian beam does not have the transverse azimuthal orbital energy flux, and therefore the transverse energy flux includes only the transverse spin flux. Therefore, they must rotate in the same direction. Below, in the final section, we show experimentally that this energy flux (orbital angular momentum) can be partially transferred to a dielectric microparticle so that it rotates relative to its center of mass.

According to Eq. (10), if circular polarization of the initial Gaussian beam changes from left-hand to right-hand, then the transverse energy flux changes its direction and rotates counterclockwise. Modeling shows that the transverse spin flux near the focus also changes its direction and rotates counterclockwise. In the experiment, this is also confirmed by counterclockwise rotation of a microparticle.

Below, based on Eqs. (7) and (11), we obtain an exact expression for the orbital angular momentum (OAM) in the focus of a Gaussian beam with left-hand circular polarization. The Poynting vector from Eq. (8) is the sum of the orbital energy flow $\mathbf{S}_{\text{or}}$ and of the spin flow $\mathbf{S}_{\text{sp}}$ [39]:

$$\mathbf{S} = \frac{\text{Re}}{2}(\mathbf{E}^* \times \mathbf{H}) = \mathbf{S}_{\text{or}} + \mathbf{S}_{\text{sp}}, \tag{12}$$

$$\mathbf{S}_{\text{or}} = \frac{\text{Im}}{2k}[\mathbf{E}^*(\nabla\mathbf{E})], \quad \mathbf{S}_{\text{sp}} = \frac{1}{4k}[\nabla \times \text{Im}(\mathbf{E}^* \times \mathbf{E})]. \tag{13}$$

For a Gaussian beam with left-hand circular polarization [Eq. (1)], Richards-Wolf theory [29] allows us to obtain expressions for the azimuthal components of the vectors $\mathbf{S}_{\text{or}}$ and $\mathbf{S}_{\text{sp}}$ via the integrals from Eq. (4):

$$\begin{aligned} S_{\text{or},\varphi} &= -\frac{1}{kr}\left(I_{1,1}^2 + I_{2,2}^2\right), \\ S_{\text{sp},\varphi} &= \frac{1}{kr}\left(I_{1,1}^2 + I_{2,2}^2\right) - I_{1,1}(I_{0,0} + I_{2,2}), \\ S_{\varphi} &= -I_{1,1}(I_{0,0} + I_{2,2}), \quad S_{\varphi} = S_{o,\varphi} + S_{s,\varphi}. \end{aligned} \tag{14}$$

Equation (14) shows that in the focal plane there is an orbital energy flux that can rotate an on-axis microparticle around its center of mass clockwise since $S_{\text{or},\varphi} = -(I_{1,1}^2 + I_{2,2}^2)/kr < 0$. It is also seen in Eq. (14) that the spin flow in the focus rotates clockwise, which is consistent with Fig. 2. Similarly to Eq. (12), the axial component J_z of the angular momentum of a light field can be written as a sum of the orbital angular momentum (OAM) L_z and of the spin angular momentum (SAM) s_{zE} [24]:

$$J_z = L_z + s_{zE} = -\frac{1}{k}\left(I_{0,0}^2 + I_{1,1}^2\right), \tag{15}$$

where

$$L_z = rP_{\text{or},\varphi} = -\frac{1}{k}\left(I_{1,1}^2 + I_{2,2}^2\right), \tag{16}$$

$$s_{zE} = \frac{1}{k}\left(I_{2,2}^2 - I_{0,0}^2\right). \tag{17}$$

As seen from Eq. (16), in the focus there is the OAM directed oppositely to the z-axis. Such OAM rotates a microparticle clockwise. From a comparison of Eqs. (16) and (17), the longitudinal projection of SAM is seen to be maximal in the focus on the optical axis. Meanwhile, the longitudinal projection of OAM is maximal on a ring of radius ∼200 nm [Fig. 1(c)]. This peculiarity of distributions of the longitudinal projections of SAM and OAM can be utilized to demonstrate a spin-orbital conversion in the strong focus. We note that similar expressions for SAM and OAM in the focus have been obtained in [40] based on the Barnett technique [41], and they are different from Eqs. (15)–(17), since the integrals (4), used in all expressions in this work, are different from similar integrals (14) in [40]. In [42], spin-orbit conversion is analyzed based on the sharp focusing of a linearly polarized Laguerre-Gaussian beam, and there are no formulas for SAM and OAM in the focus.

III. ORBITAL-SPIN CONVERSION IN THE FOCUS AND THE MÖBIUS STRIP

The energy flux of a light field can be represented as a superposition of the orbital energy flux and of the spin flux [41]. Therefore, along with the spin-orbit conversion, there must also be an inverse effect, i.e., the orbital-spin conversion. Indeed, setting $\sigma = 0$ (i.e., linear polarization) in Eq. (3), we derive an expression for the axial component of the spin density vector in the focus of an optical vortex with linear polarization directed along the X-axis:

$$s_{zE} = \tfrac{1}{2}(I_{2,m-2} - I_{2,m+2})(I_{2,m-2} + I_{2,m+2} + I_{0,m}\cos 2\varphi). \tag{18}$$

From Eq. (18) it follows that at $m = 0$ (Gaussian beam) the axial spin component (18) is absent (zero), whereas at $m = 1$ it is already nonzero:

$$s_{zE1} = \tfrac{1}{2}(I_{2,1} + I_{2,3})(I_{2,1} - I_{2,3} - I_{0,1}\cos 2\varphi). \tag{19}$$

Equation (19) demonstrates the effect of orbital-spin conversion. Indeed, at the entrance to the optical aplanatic system, a linearly polarized optical vortex has zero spin-density vector and, at the same time, a nonzero transverse energy flux due to the spiral phase. However, in the focal plane, the spin-density

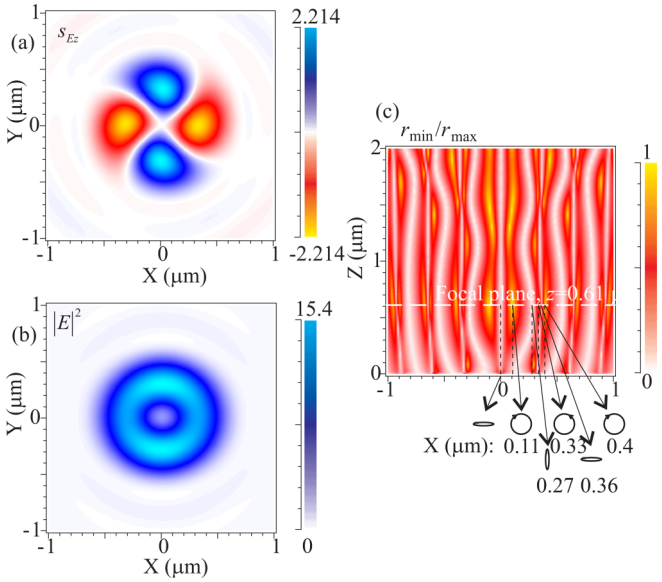

FIG. 3. Distributions of the longitudinal component s_{Ez} of the spin density (19) (a) and of the intensity $|E|^2$ (b) in the focal plane. The rightmost figure (c) shows a distribution in the XZ-plane of a minimal-to-maximal radius ratio of the 3D polarization ellipses for a focused linearly polarized Gaussian beam ($m = 0$): yellow color means C-points with circular polarization, white color means narrow ellipses, and numbers near the ellipses show the X-coordinates of their centers (in microns).

vector is nonzero and has the axial component (19), although on the axis itself ($r = 0$) the longitudinal spin component (19) is zero. Note that in this case (i.e., when the initial field is a linearly polarized optical vortex with $m = 1$), the spin-density vector [Eq. (2)] has in the focus also transverse components, which can be obtained from the general expression [Eq. (3)]. If $\varphi \approx 0$ (i.e., near the horizontal axis X), the first multiplier in Eq. (19) is positive whereas the second one is negative (since $I_{0,1} > I_{2,1}$) and thus $s_{zE1} < 0$. If $\varphi \approx \pi/2$ (near the vertical axis Y), the first multiplier in Eq. (19) is still positive but the second one is positive also (since $I_{0,1} + I_{2,1} > I_{2,3}$), and therefore $s_{zE1} > 0$. Everything written above holds near the optical axis [$kr < \gamma$, where γ is the first zero of the Bessel function $J_1(x)$].

The conclusions based on Eq. (19) are confirmed by simulation. Using the FDTD method, we calculated distributions of the axial spin component s_{Ez} [Fig. 3(a)] and of the intensity $|E|^2$ [Fig. 3(b)] in the focus of a linearly polarized optical vortex with $m = 1$. Other parameters are the same as in Fig. 1.

Figure 3(a) demonstrates that on the vertical axis (Y-axis) the longitudinal component of the spin vector (19) is directed forward along the optical axis, while on the horizontal axis (X-axis) it has the opposite direction. This means that near the vertical and horizontal transverse axes in the focal plane, the polarization vectors rotate in different directions: clockwise near the X-axis and counterclockwise near the Y-axis.

In [25], it was demonstrated both numerically and experimentally that in the longitudinal YZ-plane near the sharp focus of a linearly polarized (along the Y-axis) Gaussian beam (without the vortex, i.e., $m = 0$) there are points of circular polarization (C-points) around which the long axes of the polarization ellipses form the lemon-type polarization topology with the index of $+1/2$ and $-1/2$. In the 3D case, the surface of these polarization ellipses around the C-point forms an optical polarization Möbius strip [25,26,31]. Below we derive equations for obtaining the C-points near the focus of a linearly polarized Gaussian beam. Using the Richards-Wolf method [29] for the initial field (1) with $\sigma = 0$ (i.e., linear polarization along the X-axis), we get the electric field components expressed via the integrals (4):

$$E_x = -i(I_{0,0} + I_{2,2}\cos 2\varphi), \quad E_y = -iI_{2,2}\sin 2\varphi,$$
$$E_z = -2I_{1,1}\cos\varphi. \tag{20}$$

According to Eq. (20), the polarization ellipses on the horizontal axis (i.e., $\varphi = 0$) lie in the XZ-plane since $E_y = 0$. Therefore, it is possible to obtain an equation to find the points on the X-axis with circular polarization:

$$|E_x|^2 - |E_z|^2 = (I_{0,0} + I_{2,2})^2 - 4I_{1,1}^2 = \begin{cases} 0, & x = x_0, \\ > 0, & x < x_0, \\ < 0, & x > x_0. \end{cases} \tag{21}$$

Near the optical axis, the integral $I_{0,0}$ in Eq. (21) exceeds two other terms [since it depends on the function $J_0(x)$] and therefore the polarization ellipses are elongated along the X-axis. At some point $x = x_0$, the polarization ellipse turns into a circle (C-point), and at $x > x_0$ the polarization ellipses are elongated along the Z-axis. Such polarization topology corresponds to the lemon topology with the index of $+1/2$ [25]. Figure 3(c) shows (in pseudocolors) the small-to-large axis ratio of the 3D polarization ellipse. Centers of the ellipses are in the XZ-plane. For the FDTD-simulation, we supposed that the wavelength is $\lambda = 633$ nm, the initial field is the Gaussian beam with linear polarization along the X-axis, and that the focusing is done by a zone plate with the focal length of $f = \lambda$. As seen in Fig. 3(c), there are a number of points (yellow color) near the focus, where polarization is circular (C-points), and around which the polarization topology is of lemon-type with alternating indices $+1/2$ and $-1/2$. Coordinates of the C-points [Fig. 3(c)] are proportional to zeros of the Bessel function from Eq. (21).

In the focus, evidently, in addition to the longitudinal spin component [Eq. (19)], there are longitudinal and transverse energy fluxes:

$$S_z = \tfrac{1}{2}\left(I_{0,m}^2 - I_{2,m+2}^2 - I_{2,m-2}^2\right), \quad S_x = -Q(r)\sin\varphi,$$
$$S_y = Q(r)\cos\varphi,$$
$$Q(r) = \tfrac{1}{2}I_{1,m+1}(I_{0,m} + I_{2,m+2}) + \tfrac{1}{2}I_{1,m-1}(I_{0,m} + I_{2,m-2}). \tag{22}$$

Equation (22) shows that unlike the axial spin component [Eq. (18)], the axial component of the Poynting vector is circularly symmetric, as is the intensity distribution [Fig. 3(b)]. It is also seen from Eq. (22) that at $m = 0$ (i.e., without the optical vortex) there is no energy rotation in the focus [$Q(r) = 0$].

IV. PHOTONIC WHEELS OR PHOTONIC HELICOPTER

In the previous section, the spin density or SAM vector of a linearly polarized Gaussian beam in the focal plane is

shown to have a zero longitudinal component. However, it turns out in this case that the transverse components of the spin-density vector in the focus are nonzero. Indeed, for linear polarization along the X-axis ($\sigma = 0,\ \gamma_+ = \gamma_- = 1/\sqrt{2}$) for any m, Eq. (3) reduces to

$$\begin{aligned} s_{xE} &= \tfrac{1}{2}\sin\varphi(-I_{1,m+1}I_{2,m+2} + I_{1,m-1}I_{2,m-2}) \\ &\quad + \tfrac{1}{2}\sin 3\varphi(I_{1,m-1}I_{2,m+2} - I_{1,m+1}I_{2,m-2}), \\ s_{yE} &= \tfrac{1}{2}\cos\varphi(\sqrt{2}I_{0,m}I_{1,m+1} - \sqrt{2}I_{0,m}I_{1,m-1} \\ &\quad + I_{1,m+1}I_{2,m+2} - I_{1,m-1}I_{2,m-2}) \\ &\quad - \tfrac{1}{2}\cos 3\varphi(I_{1,m-1}I_{2,m+2} - I_{1,m+1}I_{2,m-2}), \end{aligned} \tag{23}$$

and at $m = 0$ ($s_{zE0} = 0$) we get

$$\begin{aligned} s_{xE0} &= -2\cos\varphi\sin 2\varphi I_{1,1}I_{2,2}, \\ s_{yE0} &= 2\cos\varphi\cos 2\varphi I_{1,1}I_{2,2} + \sqrt{2}\cos\varphi I_{0,0}I_{1,1}. \end{aligned} \tag{24}$$

It is seen from Eq. (24) that there is no transverse flux of the spin on the optical axis itself as well as along the vertical axis ($\varphi = \pm\pi/2$). Spin flux (24) to the right side from the vertical axis $Y(-\pi/2 < \varphi < \pi/2)$ is directed along the positive direction of this axis. According to Eq. (24), if $\varphi = 0$, then $s_{yE} = \sqrt{2}I_{1,1}(\sqrt{2}I_{2,2} + I_{0,0}) > 0$. To the left side from the vertical axis ($\pi/2 < \varphi < 3\pi/2$), the transverse spin is directed along the negative direction. If $\varphi = \pi$, Eq. (24) yields $s_{yE} = -\sqrt{2}I_{1,1}(\sqrt{2}I_{2,2} + I_{0,0}) < 0$. Since at an arbitrary point the spin vector is orthogonal to the ellipse (or circle) of rotation of the polarization vector, then, according to Eq. (24), the polarization vector to the left and to the right side from the optical axis rotates in the horizontal plane in different directions (similar to helicopter propellers). This effect is similar to the photonic wheels [24,43], but since the plane of polarization vector rotation is horizontal rather than vertical, the analogy with rotation of the helicopter propellers comes to mind. It is clear that if the plane of polarization vector rotation near the focus should be vertical (photonic wheels), it is necessary for the illuminating beam (1) to be vertically polarized (along the Y-axis) instead of horizontally (along the X-axis). We note that in [25,44] the transverse spin density was measured experimentally in the sharp focus with linear polarization. Experimentally measured s_{yE} (Fig. 3 in [44]) coincides with s_{yE} in Fig. 4(a), while measurement of the other transverse SAM density s_{xE} failed in [44] due to its small value. References [25,44] do not contain the formulas (23) and (24) describing the transverse SAM in the focus.

Figure 4 shows distributions of the transverse components of the spin-density vector (spin angular momentum) in the focus of a linearly polarized Gaussian beam (the polarization vector is directed along the X axis). Other parameters are the same as in Fig. 1. It is seen in Fig. 4 that the Y-component s_{Ey} of the spin vector exceeds more than 30 times the X-component s_{Ex} in magnitude. Thus, the s_{Ex} component can be neglected, while the shape and sign of s_{Ey} in Fig. 4(a) confirm the theoretical prediction [Eq. (24)] that the spin vector in the focal plane is oriented vertically and in the different directions at the left and at the right sides from the YZ-plane. Therefore, in the XZ-plane there are polarization ellipses (or circles) along which the electric field vector rotates in time. Such a configuration of polarization ellipses resembles the rotation of helicopter propellers [Fig. 4(c)].

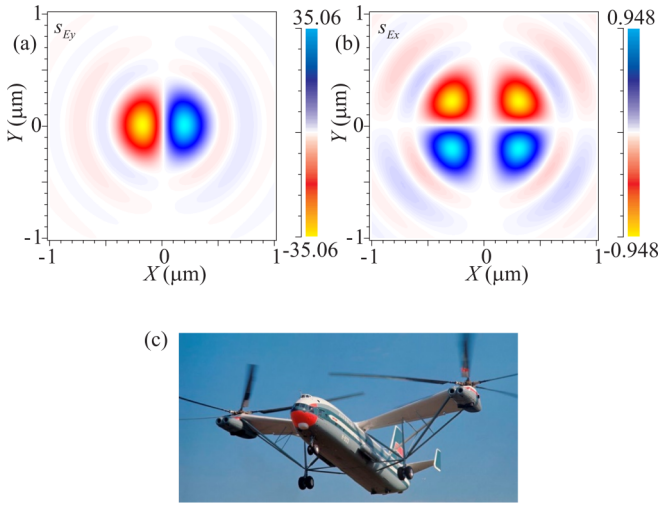

FIG. 4. Distributions of the transverse components of the spin-density vector (longitudinal component is zero) in the focal plane: s_{Ey} (a) and s_{Ex} (b). Analogy with rotation of the helicopter propellers (c).

V. PURE LONGITUDINAL SPIN IN THE FOCUS AND PURE MAGNETIZATION

An azimuthally polarized optical vortex with a topological charge m has the following complex amplitude [instead of Eq. (1)]:

$$\mathbf{E} = A(\theta)e^{im\varphi}\begin{pmatrix}-\sin\varphi\\ \cos\varphi\end{pmatrix}, \quad \mathbf{H} = A(\theta)e^{im\varphi}\begin{pmatrix}\cos\varphi\\ \sin\varphi\end{pmatrix}. \tag{25}$$

In the focal plane, components of the light field with a topological charge of $m = 1$ read

$$\begin{aligned} E_x &= -\frac{1}{2}[(I_{0,0} + I_{2,0}) + e^{i2\varphi}(I_{0,2} + I_{2,2})], \\ E_y &= -\frac{i}{2}[(I_{0,0} + I_{2,0}) - e^{i2\varphi}(I_{0,2} + I_{2,2})], \\ E_z &= 0. \end{aligned} \tag{26}$$

It is seen from Eq. (26) that the azimuthally polarized optical vortex of first order has in the focus a zero longitudinal component. Since the longitudinal component of the electric field is zero in Eq. (26), the energy flow (Poynting vector) has only a longitudinal component, while its transverse components are zero.

Then, we can obtain an expression for the longitudinal component of the spin-density vector in the plane of sharp focus:

$$s_{Ez} = \tfrac{1}{4}(|I_{0,m-1} + I_{2,m-1}|^2 - |I_{0,m+1} + I_{2,m+1}|^2). \tag{27}$$

According to Eq. (27), the effect of pure magnetization takes place [27] in this case, since in the focal plane only the longitudinal component of the spin-density vector is nonzero. The transverse components of the spin vector are zero for any m ($s_{E\varphi} = s_{Er} = 0$), and thus the plane, in which all the polarization vectors rotate, coincides with the focal plane.

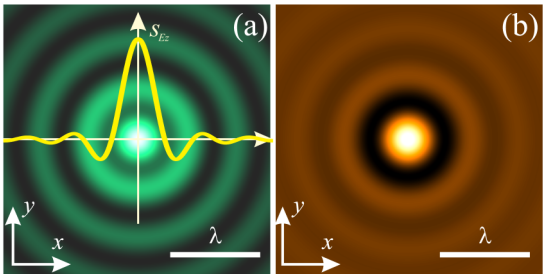

FIG. 5. Distributions of the longitudinal component of the Poynting vector S_z (black color means zero, light color means maximum) (a) and of the longitudinal component of the spin-density vector $s_{E,z}$ (black color means minimum, light color means maximum) (b) in the focal plane of a sharply focused optical vortex ($m = 1$) that passed through a narrow annular aperture. Yellow plot (a) is a section of $s_{E,z}$.

In [45], an expression is given for the longitudinal component of the Poynting vector in the focus of an optical vortex with a topological charge m and with nth-order azimuthal polarization:

$$S_z = \tfrac{1}{2}\left(I^2_{0,m+n} + I^2_{0,m-n} - I^2_{2,m+n-2} - I^2_{2,m-n+2}\right). \tag{28}$$

According to this expression, the energy flux of an azimuthally polarized ($n = 1$) optical vortex along the optical axis reads

$$S_z = \tfrac{1}{2}\left(I^2_{0,m+1} + I^2_{0,m-1} - I^2_{2,m-1} - I^2_{2,m+1}\right). \tag{29}$$

It can be shown that the axial component of the orbital energy flow (13) can be expressed via the integrals (4):

$$S_{or,z} = \tfrac{1}{4}[(I_{0,0} + I_{2,0})(J_{0,0} + J_{2,0}) + (I_{0,2} + I_{2,2})(J_{0,2} + J_{2,2})], \tag{30}$$

where

$$J_{\nu,\mu} = \left(\frac{\pi f}{\lambda}\right)\int_0^{\theta_0} \sin^{\nu+1}\left(\frac{\theta}{2}\right)\cos^{3-\nu}\left(\frac{\theta}{2}\right)\cos^{3/2}(\theta) \times A(\theta)e^{ikz\cos z}J_\mu(x)d\theta. \tag{31}$$

Equation (30) shows that on the optical axis in the focus, the orbital energy flow is maximal and positive.

Figure 5 depicts distributions of the longitudinal components of the Poynting vector S_z [Fig. 5(a)] and of the spin-density vector $s_{E,z}$ [Fig. 5(b)] in the focal plane computed using Eqs. (29) and (27). Figure 5 is obtained for the following parameters: wavelength $\lambda = 532$ nm, focal length $f = 100\lambda$, vortex order (topological charge) $m = 1$, numerical aperture NA $= \sin\theta = \sin 85 = 0.996$, calculation area $-1.5\lambda \leqslant x, y \leqslant 1.5\lambda$.

As seen in Fig. 5, the longitudinal spin component changes its sign from ring to ring in the energy flux distribution. This means that on different radii of the energy flux pattern in focus, the polarization vector rotates in different direction. On the optical axis, both the energy flux and the spin are maximal and equal, $S_{z1} = (I^2_{0,0} - I^2_{2,0})/2 > 0$ and $s_{Ez1} = |I_{0,0} + I_{2,0}|^2/4$, respectively. This can be seen from Eqs. (29) and (27) at $m = 1$ and $r = 0$.

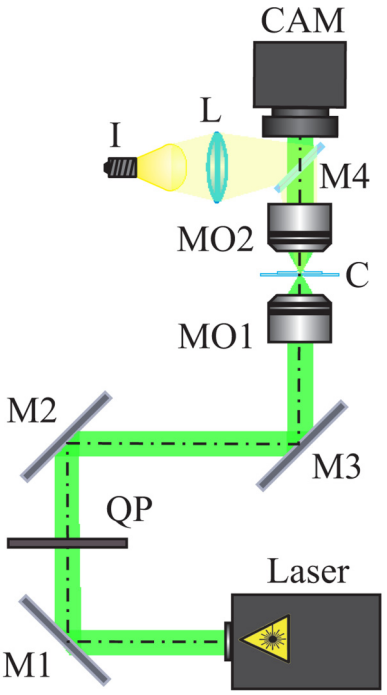

FIG. 6. Experimental optical setup for rotation of particles in a circularly polarized Gaussian beam: Laser is the solid-state laser ($\lambda = 532$ nm, $P_{\text{output}} = 100$ mW); QP is the quarter-wave plate; M1, M2, and M3 are the mirrors; MO1 and MO2 are the micro-objectives (40 ×, NA = 0.65); C is the cell with water solution with polystyrene particles; CAM is the video camera CAM (TOUPCAM UCMOS08000KPB, pixel size 1.67 μm); I is the lighting lamp; L is the biconvex lens with a focal length of 150 mm; and M4 is the semitransparent mirror.

VI. EXPERIMENTAL DEMONSTRATION OF THE SPIN-ORBITAL CONVERSION IN THE FOCUS

The experimental setup is shown in Fig. 6. A source linearly polarized laser beam of a Gaussian shape goes from a solid-state laser ($\lambda = 532$ nm, $P_{\text{output}} = 100$ mW) and then passes through a quarter-wave plate QP, which makes the beam circularly polarized. Mirrors M1, M2, and M3 direct the laser beam into the input pupil of a micro-objective MO1 (40 ×, NA = 0.65), which focuses the beam inside a cell C, formed by two coverslips and containing an aqueous solution with polystyrene particles. The focal length of the objective MO1 is 4.5 mm and the diameter of the focal spot at full width at half-maximum (FWHM) intensity is approximately FWHM $= 0.5\lambda/\text{NA} = 0.77\lambda = 0.41\,\mu$m. Micro-objective MO2 (40 ×, NA = 0.65) generates an image of the trapping plane on the matrix of a video camera CAM (TOUPCAM UCMOS08000KPB, pixel size 1.67 μm). Lamp I, lens L (focal length of 150 mm), and semitransparent mirror M4 are used for highlighting the solution with particles. Figures 7 and 8 depict experimental results on rotation of an elongated-spheroidal about (2 × 1)-μm-sized polystyrene particle in a Gaussian beam with right-hand or left-hand circular polarization.

According to Figs. 7 and 8, in the focus of a circularly polarized Gaussian beam, the spin-orbit conversion generates a spiral energy flow, as predicted by Eq. (11). Due to this

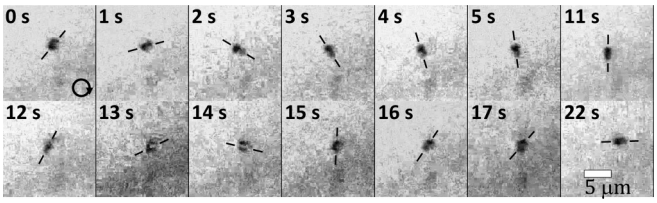

FIG. 7. Stages of rotation of a particle trapped in a focused Gaussian beam with left-hand circular polarization. Black lines show the particle orientation. The particle size is 2 by 1 μm. The size of the scale mark is 5 μm.

energy flow, a longitudinal component of the orbital angular momentum is formed in the focus of the light field, which is transmitted to the trapped microparticle and rotates it clockwise (left circular polarization) (Fig. 7) or counterclockwise (right circular polarization) (Fig. 8). Note that, according to Eq. (10), for left circular polarization the energy flux in the focus rotates clockwise, and the particle in Fig. 7 rotates clockwise, too. In addition, according to Eq. (11), for right circular polarization, the transverse energy flux in the focus rotates counterclockwise and the particle in Fig. 8 rotates counterclockwise, too.

Note that the spin-orbit conversion effect was also studied in [46–48], but those works do not contain the explicit analytical expression for the orbital angular momentum in the focus of a circularly polarized Gaussian beam. Experiments on the microparticle rotation in the focus, which demonstrate the spin-orbit conversion, are described in [47,48]. However, in [47,48], in contrast to our work, a gold (absorbing) particle was rotated rather than a dielectric (nonabsorbing) one. In addition, the gold particle was rotated in a circular path with a diameter of 10–15 μm, where the focused Gaussian beam (with a diameter of about 1 μm) has almost zero energy. In our experiment, a dielectric particle was trapped in the focus of a Gaussian beam and rotated around its center of mass. The azimuthal component of the energy flow, which rotates the particle, has its maximal value on a circle with the radius of about 0.5 μm (i.e., where the intensity drops twice in the focus [46]). Around the center of mass, spin angular momentum can rotate only an absorbing particle [49], and therefore it did not affect the dielectric nonabsorbing microparticle in our experiment.

To account for the experimental results, we have conducted numerical simulation and derived a torque exerted onto the

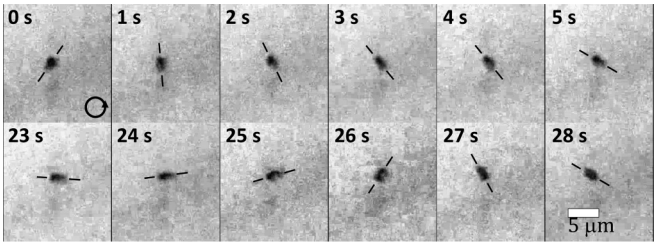

FIG. 8. Stages of rotation of a particle trapped in a focused Gaussian beam with right-hand circular polarization. Black lines show the particle orientation. The particle size is 2 by 1 μm. The size of the scale mark is 5 μm.

spheroidal microparticle of interest. Let a coherent light field fall onto a microparticle with permittivity ε_1 in a medium with permittivity ε_0. Then, an optical torque $\mathbf{M}$ exerted on the microparticle at a point A will be equal to [50,51]

$$\mathbf{M} = \oint_S [\mathbf{r} \times (\sigma \cdot \mathbf{n})] dS, \tag{32}$$

where $\mathbf{r}$ is the radius-vector drawn from the point $A(x, y, z)$ to the integration point on the surface S, $\mathbf{n}$ is the external normal vector to the surface S, A is the point relative to which the torque $\mathbf{M}$ is calculated, and σ is the Maxwell stress tensor, whose components in the CGS system can be written as [52]

$$\sigma_{ik} = \frac{1}{4\pi}\left(\frac{|\mathbf{E}|^2 + |\mathbf{H}|^2}{2}\delta_{ik} - E_i E_k - H_i H_k\right), \tag{33}$$

where E_i, H_i are the electric and magnetic field components, and δ_{ik} is the Kronecker delta ($\delta_{i=k} = 1$, $\delta_{i\neq k} = 0$). The numerical simulation was conducted for a numerical aperture of NA = 0.65, a beam power of 100 mW, a wavelength of 532 nm, and a (1 × 2)-μm spheroidal particle located in the water (refractive index $n = 1.33$). The refractive index of the particle was taken from Ref. [53] and taken to be $n = 1.6 + i0.0002$. The particle was placed in the focus of a converging left-handed circularly polarized spherical wave passing through a circular aperture, with its center found on the optical axis. The torque (32) acting on the particle center was rigorously calculated with and without regard for the imaginary part of its refractive index. With the imaginary part taken into account, the on-axis projection of the torque was equal to $M_z = 2.08 \times 10^{-19}$ N m. With the imaginary part taken to be zero (a nonabsorbing particle), the torque was found to be approximately two times smaller: $M_z = 0.82 \times 10^{-19}$ N m. This result is in good agreement with a result reported in Ref. [54], in which a spherical particle of a size equal to several wavelengths of a 514-nm Ar laser light with refractive index $n = 1.47 + i10^{-6}$ placed in the air in the focus of a circularly polarized Gaussian beam experienced a torque of $M_z = 0.3 \times 10^{-19}$ N m, causing it to rotate with an angular frequency of 4 rad/s. From Fig. 7, the particle is seen to make a half-turn per 4 s (frames from 11th to 15th second), hence the experimental angular rotation frequency is about $\omega = \pi/4$rad/s. This is the maximum rotation frequency achieved by the particle in Fig. 7. The Stokes formula for a drag torque [30] is $M_{\mathrm{drag},z} = -8\pi\eta a^3\omega$, where a is the radius of a spherical particle and η is the fluid viscosity. In our experiment with a (2 × 1)-μm particle, we assume $a = 1.41 \times 10^{-6}$ m. At room temperature, the water viscosity is $\eta = 0.00089$ Ns/m^2. Then, we find that $M_{\mathrm{drag},z} = 0.49 \times 10^{-19}$ N m, which is less than the torque derived for a nonabsorbing particle ($M_z = 0.82 \times 10^{-19}$ N m). For an absorbing particle, the rotation frequency would be four times higher than that measured in the experiment. By way of illustration, the relationship derived in Ref. [49] for a spherical particle gives a rotation frequency of $\omega = IM_g M'M''/[\eta c(M'^2 + 2)] = 5$ rad/s, where $M' = \mathrm{Re}(n)$, $M'' = \mathrm{Im}(n)$, I is the intensity of light (W/m^2), M_g is the refractive index of the medium (for water, $M_g = 1.33$), and c is the velocity of light in vacuum. This is an overestimated value for the rotation frequency, because the relationship is valid for the Rayleigh particles whose

radius is much less than the incident wavelength. This is approximately the same frequency at which strongly absorbing particles would have rotated when trapped in the beam. For example, a 2-μm CuO particle has been described to rotate with a 4-Hz frequency along a circular path in kerosene ($\eta = 1.58 \times 10^{-3}$ N s/m^2) when trapped in a 10-mW beam [30]. In another study [31], 1–5-μm CuO particles were reported to rotate with an ∼1-Hz frequency in a 633-nm laser beam of 17-mW power that passed through an aperture with NA = 1.3. Experimental results most similar to ours were reported in Ref. [55] on trapping a 1-μm Teflon sphere with a 2% absorption in a 25-mW laser beam of wavelength 1064 μm (NA = 1.3), which rotated around its center of masses with a ∼1-Hz frequency (2π rad/s). However, it is important to mention that absorption of a Teflon particle is an order of magnitude higher than that of a polystyrene particle in our experiment, resulting in the rotation frequency of the polystyrene particle being almost an order of magnitude less ($\pi/4$ rad/s).

Summing up, a rigorous calculation of the torque exerted on a particle under near-experimental conditions has shown that with the particle absorption taken into account, the resulting torque is nearly twice as high. Meanwhile, the theoretically calculated rotation frequency is several times higher than that observed in the experiment. This may be because the particle got trapped prior to the focus where the gradient focus-directed upward force (Fig. 6) was compensated for by the gravity force. Let us remember that with increasing distance from the focus, the torque sharply decreases [54]. Our dielectric weakly absorbing microparticle was observed to rotate about its axis near the focus of a Gaussian beam, unlike all other known experiments, in which particles were reported to rotate in an annular laser beam [30,31,47,48,55].

We also calculated torques exerted on a 200-nm on-axis spherical particle ($n = 1.6 + i0.0002$) placed in water in the focal plane (NA = 0.65): $M_z = 0.3 \times 10^{-19}$ N m. If the spherical particle was shifted from the axis by 300 nm, the torque applied to its center became zero (having reduced by two orders of magnitude), with the particle ceasing to rotate about its axis. In the meantime, the torque relative to the optical axis exerted on the off-axis particle was found to increase by a factor of 2.5: $M_z = 0.8 \times 10^{-19}$ N m. Therefore, we can infer that a 200-nm off-axis particle would move around the optical axis along a spiral path, being attracted to where the on-axis intensity is maximal. This calculation substantiates the feasibility of demonstrating the individual effect of OAM and SAM on the particle in the strong focus.

VII. CONCLUSION

Here, we have obtained the following results. Based on the Richards-Wolf theory, analytical expressions have been obtained for the energy flux and for the spin density in the sharp focus of vortex laser beams with linear, circular, and azimuthal polarization. Using the obtained expressions, the following optical phenomena have been shown to take place in the focus.

Spin-orbital conversion. A source circularly polarized Gaussian beam does not have the orbital angular momentum (OAM), but in the plane of sharp focus the OAM of such a beam is nonzero (that is, there is a transverse energy flux). The transverse energy flux in the focus is equal in magnitude and in sign to the transverse spin flux for both left-hand and right-hand circular polarization. Both fluxes (spin flux and energy flux) rotate near the focus clockwise (for left-hand circular polarization of the Gaussian beam) and counterclockwise (for right-hand circular polarization of the Gaussian beam). In our experiment, a circularly polarized laser beam with a wavelength of 532 nm and a power of 100 mW was focused with a numerical aperture of 0.65. We demonstrated the rotation of a polystyrene spheroidal (1×2) μm microparticle around its center of mass and around the optical axis (half revolution in 4 s). A change in the handedness of circular polarization of the Gaussian beam led to a change in the direction of microparticle rotation.

Orbital-spin conversion. A linearly polarized optical vortex with unit topological charge does not have the spin vector, but in the area of sharp focus an axial spin-density vector appears, and it is distributed in the focal plane so that the polarization vector rotates differently in different areas: clockwise near the horizontal transverse axis and counterclockwise near the vertical axis. The spin vector on a certain-radius circle (350 nm) in the focal plane forms in this case the Möbius strip.

Photonic wheels or helicopter propellers. In the plane of sharp focus, the spin-density vector of a linearly polarized Gaussian beam has only transverse components (its longitudinal component is zero). If linear polarization of the initial beam is horizontal, then in the focal plane the spin-density vector is directed vertically, that is, the polarization ellipses lie in the horizontal plane, and the polarization vectors in these ellipses rotate in different directions at different sides from the optical axis (clockwise and counterclockwise). This rotation of the polarization vectors in the horizontal plane resembles the rotation of helicopter propellers.

The effect of pure magnetization. An azimuthally polarized optical vortex with an integer topological charge has no spin. But in the plane of sharp focus, a spin-density vector (or spin angular momentum) appears, directed along the optical axis. There are no transverse components of the spin vector. This means that the polarization ellipses are in the focal plane. The rotation direction of the polarization vectors (clockwise or counterclockwise) in the focal plane alternates from ring to ring of the diffraction pattern in the beam cross section.

ACKNOWLEDGMENTS

The work was funded by the Russian Foundation for Basic Research under Grant No. 18-29-20003 (section "Orbital-spin conversion in the focus and the Möbius strip") and Russian Science Foundation under Grant No. 18-19-00595 (all other theoretical sections and the experiment); sections "Introduction" and "Conclusion" were supported by RF Ministry of Science and Higher Education.

[1] T. Grosjean and I. Gauthier, Opt. Commun. **294**, 333 (2013).
[2] Z. Wu, K. Zhang, S. Zhang, Q. Jin, Z. Wen, L. Wang, L. Dai, Z. Zhang, H. Chen, G. Liang, Y. Liu, and G. Chen, Opt. Express **26**, 16585 (2018).
[3] J. Guan, J. Lin, C. Chen, Y. Ma, J. Tan, and P. Jin, Opt. Commun. **404**, 118 (2017).
[4] T. Liu, J. Tan, and J. Liu, Opt. Commun. **294**, 21 (2013).
[5] N. Bokor and N. Davidson, Opt. Commun. **279**, 229 (2007).
[6] Y. Yu, H. Huang, M. Zhou, and Q. Zhan, Opt. Commun. **407**, 398 (2018).
[7] C. Zheng, S. Su, H. Zang, Z. Ji, Y. Tian, S. Chen, K. Mu, L. Wei, Q. Fan, C. Wang, X. Zhu, C. Xie, L. Cao, and E. Liang, Appl. Opt. **57**, 3802 (2018).
[8] J. Lin, R. Chen, P. Jin, M. Cada, and Y. Ma, Opt. Commun. **340**, 69 (2015).
[9] Y. Yu and Q. Zhan, J. Opt. **17**, 105606 (2015).
[10] H. Chen, S. Tripathi, and K. C. Toussaint, Opt. Lett. **39**, 834 (2014).
[11] C. Ping, Ch. Liang, F. Wang, and Y. Cai, Opt. Express **25**, 32475 (2017).
[12] K. Prabakaran, R. Chandrasekaran, G. Mahadevan, Z. Jaroszewicz, K. B. Rajesh, and T. V. S. Pillai, Opt. Commun. **295**, 230 (2013).
[13] V. V. Kotlyar, A. A. Kovalev, and A. G. Nalimov, Opt. Lett. **43**, 2921 (2018).
[14] V. V. Kotlyar, S. S. Stafeev, and A. A. Kovalev, Opt. Express **27**, 16689 (2019).
[15] V. V. Kotlyar, A. A. Kovalev, and A. P. Porfirev, Phys. Rev. A **97**, 053833 (2018).
[16] V. V. Kotlyar, A. G. Nalimov, and S. S. Stafeev, J. Opt. Soc. Am. B **36**, 2850 (2019).
[17] O. G. Rodriguez-Herrera, D. Lara, K. Y. Bliokh, E. A. Ostrovskaya, and C. Dainty, Phys. Rev. Lett. **104**, 253601 (2010).
[18] B. Roy, N. Ghosh, S. Dutta Gupta, P. K. Panigrahi, S. Roy, and A. Banerjee, Phys. Rev. A **87**, 043823 (2013).
[19] B. Roy, N. Ghosh, A. Banerjee, S. D. Gupta, and S. Roy, New J. Phys. **16**, 083037 (2014).
[20] P. Meng, Z. Man, A. P. Konijnenberg, and H. P. Urbach, Opt. Express **27**, 35336 (2019).
[21] W. T. M. Irvine and D. Bouwmeester, Nat. Phys. **4**, 716 (2008).
[22] D. Sugic and M. R. Dennis, J. Opt. Soc. Am. A **35**, 1987 (2018).
[23] H. Larocque, D. Sugic, D. Mortimer, A. J. Taylor, R. Fickler, R. W. Boyd, M. R. Dennis, and E. Karimi, Nat. Phys. **14**, 1079 (2018).
[24] A. Aiello, P. Banzer, M. Neugebauer, and G. Leuchs, Nat. Photon. **9**, 789 (2015).
[25] T. Bauer, M. Neugebauer, G. Leuchs, and P. Banzer, Phys. Rev. Lett. **117**, 013601 (2016).
[26] T. Bauer, P. Banser, E. Karimi, S. Orlov, A. Rubano, L. Marrucci, E. Santamato, R. W. Boyd, and G. Leuchs, Science **347**, 964 (2015).
[27] Y. Jiang, X. Li, and M. Gu, Opt. Lett. **38**, 2957 (2013).
[28] S. Zhang, S. Fu, H. Zhang, X. Ge, Z. Bai, Y. Lyu, R. Zhao, and Z. Man, Opt. Express **27**, 33621 (2019).
[29] B. Richards and E. Wolf, Proc. R. Soc. London, Ser. A **253**, 358 (1959).
[30] H. He, M. E. J. Friese, N. R. Heckenberg, and H. Rubinsztein-Dunlop, Phys. Rev. Lett. **75**, 826 (1995).
[31] M. E. J. Friese, J. Enger, H. Rubinsztein-Dunlop, and N. R. Heckenberg, Phys. Rev. A **54**, 1593 (1996).
[32] R. Martinez-Herrero and P. M. Mejias, Opt. Express **18**, 7965 (2010).
[33] K. Y. Bliokh, M. A. Alonso, E. A. Ostrovskaya, and A. Aiello, Phys. Rev. A **82**, 063825 (2010).
[34] P. B. Monteiro, P. A. Maia Neto, and H. M. Nussenzveig, Phys. Rev. A **79**, 033830 (2009).
[35] K. Y. Bliokh, A. Y. Bekshaev, and F. Nori, Nat. Commun. **5**, 3300 (2014).
[36] K. S. Youngworth and T. G. Brown, Opt. Express **7**, 77 (2000).
[37] V. V. Kotlyar, S. S. Stafeev, A. G. Nalimov, M. V. Kotlyar, L. O'Faolain, and E. S. Kozlova, Opt. Express **25**, 19662 (2017).
[38] V. V. Kotlyar, S. S. Stafeev, A. G. Nalimov, and L. O'Faolain, Appl. Phys. Lett. **114**, 141107 (2019).
[39] M. V. Berry, J. Opt. A **11**, 094001 (2009).
[40] M. Li, Y. Cai, S. Yan, Y. Liang, P. Zhang, and B. Yao, Phys. Rev. A **97**, 053842 (2018).
[41] S. M. Barnett, J. Opt. B **4**, S7 (2002).
[42] S. Nechayev, J. S. Eismann, G. Leuchs, and P. Banzer, Phys. Rev. B **99**, 075155 (2019).
[43] P. Banzer, M. Neugenbauer, A. Aiello, C. Marquardt, N. Lindlein, T. Bauer, and G. Leuchs, J. Eur. Opt. Soc. Rap. Public. **8**, 13032 (2013).
[44] M. Neugebauer, T. Bauer, A. Aiello, and P. Banzer, Phys. Rev. Lett. **114**, 063901 (2015).
[45] V. V. Kotlyar, S. S. Stafeev, and A. A. Kovalev, Comput. Opt. **43**, 337 (2019).
[46] T. A. Nieminen, A. B. Stilgoe, N. R. Heckenberg, and N. Rubinsztein-Dunlop, J. Opt. A **10**, 115005 (2008).
[47] Y. Zhao, J. S. Edgar, G. D. M. Jeffries, D. McGloin, and D. T. Chiu, Phys. Rev. Lett. **99**, 073901 (2007).
[48] Y. Zhao, D. Shapiro, D. McGloin, D. T. Chiu, and S. Marchesini, Opt. Express **17**, 23316 (2009).
[49] P. L. Marston and J. H. Crichton, Phys. Rev. A **30**, 2508 (1984).
[50] C. Rockstuhl and H. P. Herzig, Opt. Soc. Am. A **22**, 109 (2005).
[51] F. G. Mitri, J. Opt. Soc. Am. A **34**, 1246 (2017).
[52] L. D. Landau and E. M. Lifshitz, *The Classical Theory of Fields* (Pergamon, Oxford, 1973).
[53] A. Shahin, W. Bachir, and M. S. El-Daher, J. Spectrosc. **2019**, 3406319 (2019).
[54] S. Chang and S. S. Lee, J. Opt. Soc. Am. B **2**, 1853 (1985).
[55] N. B. Simpson, K. Dholakia, L. Allen, and M. J. Padgett, Opt. Lett. **22**, 52 (1997).